

DOI: 10.1515/amm-2017-0030

H.A. ALBRITHEN*, **, ***, M. ELNAGGAR*, ****, *****#, K. OZGA*****#, M. SZOTA*****#, Z.A. ALAHMED*, A.Q. ALANAZI*, H. ALSHAHRANI*, E.ALFAIFI*, M.A. DJOUADI*****#, J.P. LABIS**

STRUCTURAL TRANSITION IN SrZnO LASER PULSE DEPOSITED ALLOY

We have discovered a structural transition for the SrZnO alloy films from a wurtzite to a rock-salt structure, leading to a reduction in the (1120)/(0001) surface energy ratio. The films were grown by pulsed laser deposition using different SrO ratios, x . We have revealed that growth at a higher temperature, 750°C, resulted in a sharp 0002 peak at a low SrO content (5%), whereas growth at a higher SrO content (10%) resulted in a non-crystalline film with minute crystallites with a (1120) orientation. Generally the crystallinity decreased as the SrO content increased. No results obtained for the crystalline films showed any orientation of significant peaks besides the peak attributed to the (0001) plane, suggesting epitaxial growth. Optical measurements showed difference in transmission widows of alloys with different SrO percentage, and this was correlated to SrO influence on growth mode as indicated by scanning electron imaging. The studied SrZnO films, with $\text{SrO}/(\text{SrO} + \text{ZnO}) \leq 0.25$, were grown by pulsed laser deposition using different SrO ratios, x . The effects of temperature and oxygen pressure during growth on the films' structural properties were investigated. XRD results indicate that the film crystallinity was improved as the temperature and O₂ pressure increased up to 650°C and 0.5 Torr, respectively.

Keywords: oxide materials, solid state alloys, structural phase transitions, X-ray diffraction, scanning electron microscopy.

1. Introduction

Zinc oxide and their solid state alloys has gained much interest due to its perspective physical properties, such as non-linear optical, piezoelectric, piezooptics etc., such the ability to be synthesized using different methods [1]. To modify the properties of ZnO while maintaining the compound's wurtzite structure, many research groups have tried to dope this material with different elements possessing an electronic configuration similar to that of zinc. This process usually leads to dopants substituting into Zn lattice sites, resulting in a variation in the lattice parameters and electronic structure of Zn and thus affecting the magnitude of the material's band gap. Over-doping, in many cases, leads to a phase change from wurtzite to another phase, depending on the dopant. Previous studies [2-22] show that the main dopants that create such an effect are Be, Mg, and Cd, Ca. Doping with Be has indicated that the solubility of Be in ZnO is nearly 100%, resulting in band-gap widening. Similar behavior has been observed for Mg dopants; however, the solubility is limited to approximately 35%, beyond which the alloy undergoes a phase change to a rock-salt structure. On the other

hand, doping with Cd has been reported to reduce the band gap of ZnO, as demonstrated by [10] for up to ~7% Cd incorporation. Alloying ZnO with either Mg or Cd results in a slight variation in the lattice parameters of ZnO. Of course, the use of Be and Cd materials is not favorable due to their high toxicity and thus negative impact on health and the environment. This problem encourages the consideration of other elemental dopants with the same outer electronic structure.

Considering other alternatives leads to the group below Mg in the periodic table, namely, calcium, strontium, and barium. Compared with the aforementioned elements (Be, Mg, and Cd), Ca, Sr, and Ba have been the subject of much fewer studies; consequently, there are few reports on the alloys CaZnO, SrZnO, and BaZnO, with most focusing on CaZnO. Both experimental work and DFT calculations [23-25] show that the band gap of CaZnO increases as the content of Ca increases. CaZnO has been reported [26-28] to be synthesized by wet chemistry and RF magnetron sputtering. In [28] reported the use of RF magnetron sputtering to grow the aforementioned alloys (CaZnO, SrZnO, and BaZnO) as components of Love wave sensors; the authors observed distinct changes in the operating characteristics of the sensors as

* PHYSICS AND ASTRONOMY DEPARTMENT, COLLEGE OF SCIENCE, KING SAUD UNIVERSITY, P.O. BOX 2455, RIYADH 11451, SAUDI ARABIA

** KING ABDULLAH INSTITUTE FOR NANOTECHNOLOGY, KING SAUD UNIVERSITY, RIYADH, SAUDI ARABIA

*** NATIONAL CENTER FOR NANOTECHNOLOGY, KING ABDULAZIZ CITY FOR SCIENCE AND TECHNOLOGY, RIYADH, SAUDI ARABIA

**** RESEARCH CHAIR OF EXPLOITATION OF RENEWABLE ENERGY APPLICATIONS IN SAUDI ARABIA, PHYSICS AND

***** PHYSICS DEPARTMENT, FACULTY OF SCIENCE, AIN SHAMS UNIVERSITY, 11566 ABASSIA, CAIRO, EGYPT

***** CZESTOCHOWA UNIVERSITY OF TECHNOLOGY, INSTITUTE OF ELECTRONIC AND CONTROL SYSTEM, 17 ARMII KRAJOWEJ AV., 42-200 CZESTOCHOWA, POLAND

***** CZESTOCHOWA UNIVERSITY OF TECHNOLOGY, INSTITUTE OF MATERIAL SCIENCE ENGINEERING, 19 ARMII KRAJOWEJ AV., 42-200 CZESTOCHOWA, POLAND

***** INSTITUT DES MATERIAUX JEAN ROUXEL (IMN - UNIVERSIT'E DE NANTES, UMR CNRS 6502), 2 RUE DE LA HOUSSINIERE, BP 92208, 44322 NANTES CEDEX 3, FRANCE

Corresponding author: Cate.Ozga@wp.pl

the dopant concentration or type was varied. The concentration of the dopants they used did not exceed 5%. The authors also observed that other XRD peaks besides the main (0002) peak began to appear as the doping level was increased. From a thermodynamics perspective, [26-27] showed that the solubility of Ba in a ZnO matrix is very limited. All reports have indicated a slight variation in the lattice constants of CaZnO, SrZnO, and BaZnO, quite similar to the cases of MgZnO and CdZnO.

In this study, SrZnO alloys grown on Al₂O₃(0001) using pulsed laser deposition (PLD) were examined by XRD. In particular, the study focused on the effects of temperature and oxygen background pressure during film growth on the crystalline properties and growth modes of the alloy films in order to reveal an occurrence of phase transitions.

2. Materials and Methods

Samples were grown on Al₂O₃ (0001) substrates; the substrates were cleaned using solvents, mainly ethanol, prior to their placement in the PLD chamber to remove any contamination. The chamber, produced by Neo Cera, is equipped with a 248 nm excimer laser. Before growth, the substrates were heated to 750°C under vacuum inside the chamber to further clean the substrates and smooth their surfaces. The background gas used was oxygen, O₂; no other gases were intentionally added. Films were grown by applying laser pulses to targets measuring 2" in diameter. Three targets composed of a mixture of SrO and ZnO – with SrO molar ratios, $x = \text{SrO}/(\text{SrO} + \text{ZnO})$, equal to 5%, 10%, and 25% – were used. The pulse fluence and repetition rate were 6.5 to 7 J/cm² and 10 Hz, respectively. The films were grown at low and high temperature and under low and high oxygen background pressure as well.

To characterize the structural properties of the prepared SrZnO films, 2θ scan measurements were performed using a computer-aided, high-resolution XRD system (X'Pert Pro (MRD) from Panalytical) with CuK_α radiation ($\lambda = 1.541 \text{ \AA}$). The system is equipped with a high-resolution goniometer with a minimum 2θ step size of 0.0001°. Optical transmission in UV-Vis-IR regime was used to investigate the optical properties, and imaging by SEM was utilized to explore films structure.

3. Results and discussion

Fig. 1 shows the XRD spectra of two samples grown with different SrO molar ratios, $x = 5$ and 10%, as well as the XRD spectrum of a pure substrate for comparison. These samples were grown at 380°C under an O₂ background pressure of 15 mTorr. The spectrum shows a small (0002) peak for the alloy containing 5% SrO, whereas the sample containing 10% SrO does not exhibit an apparent peak. Moreover, no other orientations of the films were observed; the only peaks that appeared were those due to the substrate. This result, in fact, indicates the amorphous character of the alloy containing 10% SrO.

For growth at higher temperature, three Sr_xZn_{1-x}O alloys with different values of x were examined. Fig. 2 presents the XRD spectra of three samples, with $x = 5, 10,$ and 25%, as well as the spectrum of a pure substrate. The growth temperature was 650°C, whereas a background pressure of 15 mTorr was maintained. Growth behavior similar to that exhibited at 380°C was observed; however, the (0002) peak of the alloy with $x = 5\%$ became more distinct, and the intensity ratio of this peak to the substrate peak was enhanced. The other samples with higher SrO ratios ($x = 10\%$ and 25%) did not show any evidence of ordering. This result suggests the limitation of SrO miscibility in ZnO. However, the growth conditions contribute to the kinetics of this alloy's solubility limits. These results call attention to the investigation of growth parameters other than temperature. The data, shown next, presents the effect of the O₂ background pressure on the crystallinity of the films.

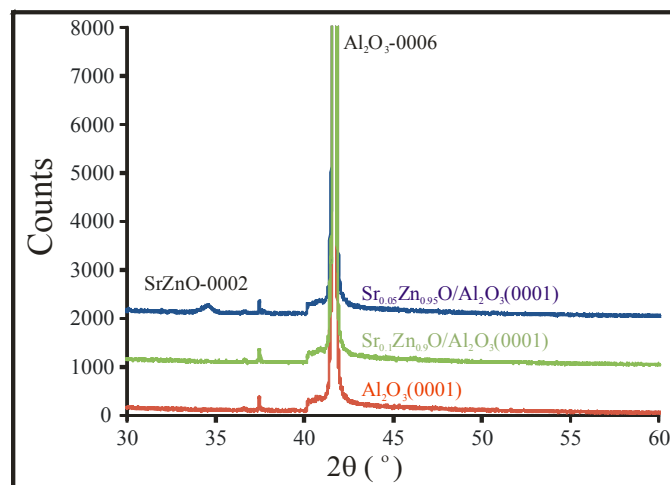


Fig. 1. XRD spectra of Al₂O₃(0001) and Sr_{0.05}Zn_{0.95}O and Sr_{0.1}Zn_{0.90}O grown on Al₂O₃(0001) at T = 380°C under 15 mTorr O₂ background pressure

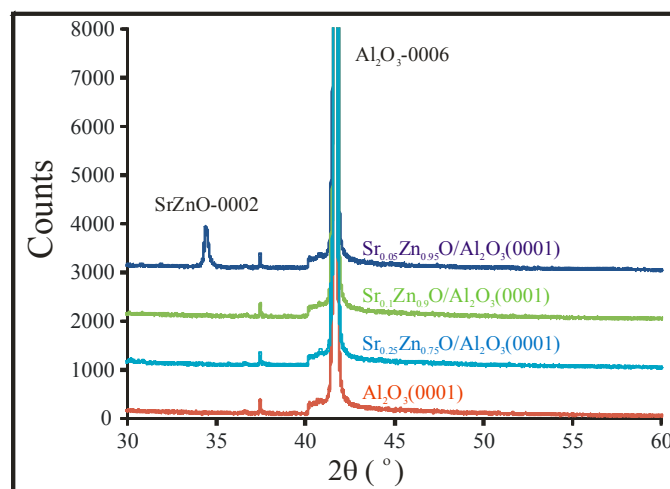


Fig. 2. XRD spectra of Al₂O₃(0001) and Sr_{0.05}Zn_{0.95}O, Sr_{0.1}Zn_{0.90}O, and Sr_{0.25}Zn_{0.75}O grown on Al₂O₃(0001) at T = 650°C under 15 mTorr O₂ background pressure

Fig. 3 shows the XRD spectra of SrZnO alloys grown at 650°C and 500 mTorr. None of the peak positions of the alloys shows significant variation from those of pure ZnO; moreover, no other peaks, except those due to the substrate, were observed, indicating a single orientation. Compared with the films grown at lower temperature or pressure, the resultant films exhibited better crystalline ordering. Indeed, a similar observation was reported by [29] for the case of pure ZnO grown by PLD on sapphire (0001). The author reported that growth at higher temperature and pressure enhances the quality of the films.

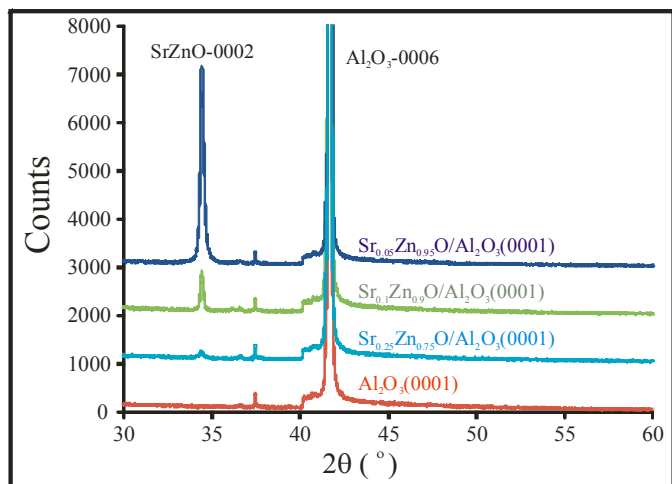


Fig. 3. XRD spectra of $\text{Al}_2\text{O}_3(0001)$ and $\text{Sr}_{0.05}\text{Zn}_{0.95}\text{O}$, $\text{Sr}_{0.1}\text{Zn}_{0.9}\text{O}$, and $\text{Sr}_{0.25}\text{Zn}_{0.75}\text{O}$ grown on $\text{Al}_2\text{O}_3(0001)$ at $T = 650^\circ\text{C}$ under 0.5 Torr O_2 background pressure

In fact, the variation in the peak positions as a function of the growth conditions or SrO concentration was not significant. Consequently, the vertical lattice constant, c , did not change considerably. Similar behavior, but not exactly the same, has been observed for Zn-rich MgZnO and CdZnO alloys exhibiting a wurtzite phase. For Zn-rich MgZnO, the change in the a -lattice (c -lattice) constant has been reported [15] to be $\sim +0.4\%$ (-0.5%) for a MgO concentration of 34%. Moreover, Zn-rich CdZnO alloy shows a similarly small variation, although the phase stability of the wurtzite phase of this alloy is lower than that of MgZnO, reaching up to $\sim 7.5\%$ as shown by [11]. According to the density functional calculations performed by [30], SrO can adopt a metastable, hexagonal structure. However, this hexagonal structure has an internal parameter (u) equal to 0.5. The same behavior is observed for MgO, whose metastable structure is called h -MgO. Based on this calculated prediction, the small variation in the lattice parameters, and the XRD peak positions, it can be assumed that the same effect occurs in MgZnO [31]. As shown in Fig. 4 the variation in the (0002) peak position of SrZnO and the alloy's c -lattice constant are very small. By converting the peak positions to lattice constants as shown in Fig. 4b, the lattice constants can be observed to increase with the SrO ratio in the SrZnO films. However, this variation in the lattice constant is very minute, similarly to the cases of MgZnO and CdZnO. In fact, other research groups have also reported small

variations in the lattice constants of ZnO-rich CaZnO, BaZnO, and SrZnO films. These small variations have been attributed to the additional stress induced by the difference in the atomic radii of Ca, Ba, and Sr and the atomic radius of Zn.

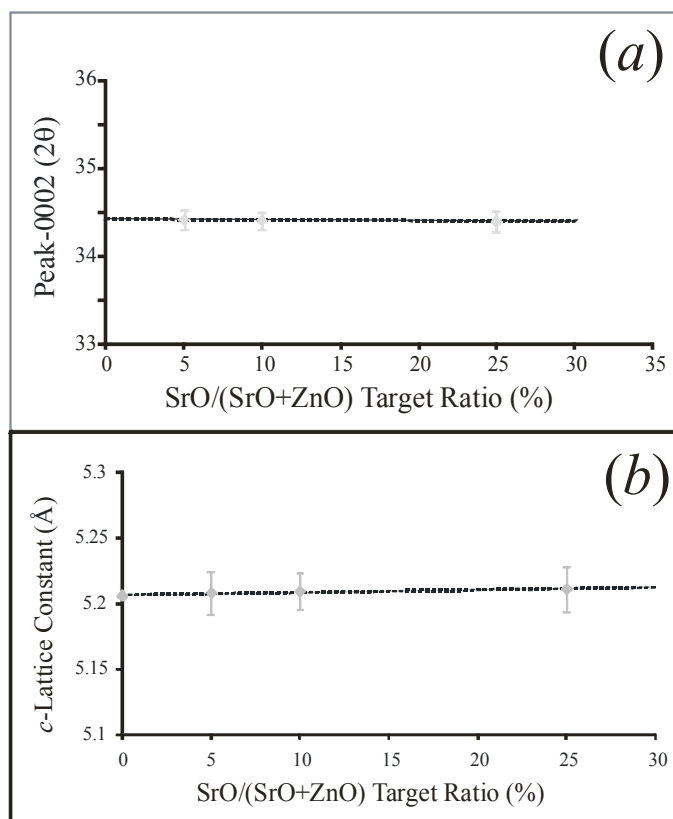


Fig. 4. Peak positions and c -lattice constants of SrZnO alloy as a function of SrO ratio (x)

Unlike in other studies, SrZnO, CaZnO, and BaZnO were grown on sapphire rather than quartz or glass plates in our study. Moreover, the method used was PLD rather than chemical bath deposition, sputtering, and sol-gel processing. For growth by a wet chemistry process, it has been demonstrated that as the contents of Ca, Sr, and Ba in the bulk increase, other orientation peaks will arise, indicating a reduction in the surface energy ratio between the (0001) orientation and other ones. Furthermore, the growth kinetics allow for such orientated growth. However, for the case of sputtering, only the (0001) orientation has been observed.

To test optical properties of those films showing strong 0002-peaks (5% SrO and 10% SrO), transmission measurements have been performed. Fig. 5 provides both transmission spectra of films with 5% SrO (Fig. 5a) and 10% SrO (Fig. 5b). For the film of 5% SrO, the behavior of the transmission spectrum has no major difference of that of pure ZnO, but transmission spectrum of film containing 10% SrO has a major shift in the transparent window. Moreover, reduction in transmission, as clearly observed, is not as sharp as that of the film containing 5% SrO. In fact one might think of band gap widening due to Sr incorporation yet this shift is not seen for the case in Fig. 5a. Indeed if

this major shift was related to electronic structure modification due to 10% SrO incorporation, a similar trend would be seen for the case of 5% SrO as well. However, the case is not so. This in fact required us to investigate how SrO influence the growth mode of the alloy, and this may explain this optical behavior.

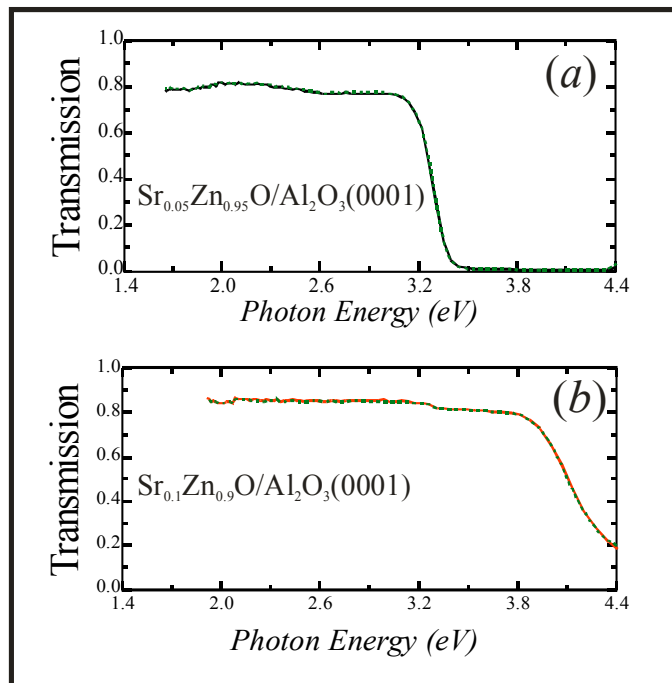


Fig. 5. Transmission spectra of a) $\text{Sr}_{0.05}\text{Zn}_{0.95}\text{O}/\text{Al}_2\text{O}_3(0001)$; and b) $\text{Sr}_{0.1}\text{Zn}_{0.9}\text{O}/\text{Al}_2\text{O}_3(0001)$. Both films were grown at $T = 650^\circ\text{C}$ under 0.5 Torr O_2 background pressure

Fig. 6 shows the images of both samples whose optical transmission spectra are presented in 5% SrO (Fig. 6a) and 10% SrO (Fig. 6b). As can be seen ZnO with 5% SrO consists of a layer with nano hexagonal rods, having a width of 100 nm. However, the case for ZnO with 10% SrO is totally different; this film is constructed of wide and thin intersecting hexagons (width is $\sim 200\text{--}300$ nm) rather than rods. This is in fact very interesting to show how SrO incorporation can have an influence on the growth mode of the alloy.

In deed this difference in growth mode explains very well the difference in the transmission spectra. For the case of SrZnO alloy of 5% SrO, the layer prevents transmission above the bandgap, and this is why no transmission is observed above ~ 3.4 eV. On the other hand, SrZnO ally of 10% SrO has a wider transmission window due to variation of band gap since thicknesses of the hexagons are not uniform. Therefore, each thickness has different electron and hole levels in the conduction and valence bands, respectively. Of course the small thickness leads to charge carrier confinement causing induction of discrete levels. Therefore, the variation of these hexagon thicknesses can be seen in the transmission spectrum, i.e. the thinner the hexagon the larger the gap, and vice versa. Indeed, further theoretical and experimental investigation is required to understand the origin of SrO percentage on SrZnO growth mode.

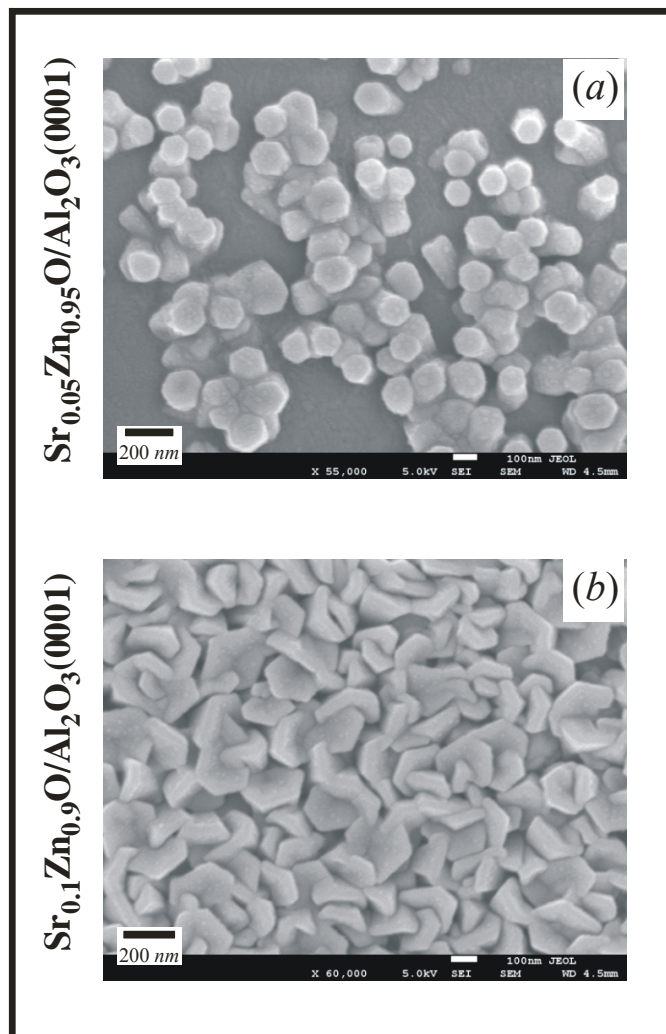


Fig. 6. Scanning electron microscopy images of a) $\text{Sr}_{0.05}\text{Zn}_{0.95}\text{O}/\text{Al}_2\text{O}_3(0001)$; and b) $\text{Sr}_{0.1}\text{Zn}_{0.9}\text{O}/\text{Al}_2\text{O}_3(0001)$. Both films were grown at $T = 650^\circ\text{C}$ under 0.5 Torr O_2 background pressure

To test the films at higher temperature, another set of samples were grown at 750°C ; the SrO bulk ratios in the targets were 5% and 10% under an O_2 pressure of 500 mTorr. The XRD spectrum of the sample containing 5% SrO (Fig. 7) shows a significant (0002) peak, indicating a high-quality film. However, for the higher SrO ratio (10%), no peak near 34.5° was observed, indicating an amorphous structure. However, a very small peak near $2\theta = 56.9^\circ$ was observed, which can be attributed to small, (11 $\bar{2}$ 0)-oriented crystals within the amorphous film. The fact that the orientation observed is different from the (0001) orientation could be related to that the fact that the (0001) surface of SrZnO alloy containing 10% SrO has a higher surface energy than the (11 $\bar{2}$ 0) surface. Indeed, it is no surprise that such a result was observed because pure SrO stabilizes in a rock-salt structure, whereas ZnO stabilizes in a wurtzite structure. Therefore, incorporating more SrO into the ZnO matrix can cause deformation, leading to a transformation from a hexagonal to a cubic phase; however, with only 10% SrO, the alloy would suffer from issues regarding its transitional state. One of these issues is the change in surface energy. The (11 $\bar{2}$ 0) surface of ZnO is rectangular in

shape with unit cell dimensions of $5.2 \text{ \AA} \times 5.5 \text{ \AA}$. These dimensions are similar to those of the square surface unit cell of SrO, which has the lowest surface energy among rock-salt structures. In fact, the a -lattice constant of rock-salt SrO is approximately 5.1 \AA , which is similar to the a -lattice parameter of wurtzite ZnO (11 $\bar{2}$ 0) reported by [30]. The reason this behavior is observed at high temperature but not at low temperature is that the thermodynamics in the former case overcome the kinetics of growth, which explains why this orientation was not observed at low temperature in this study.

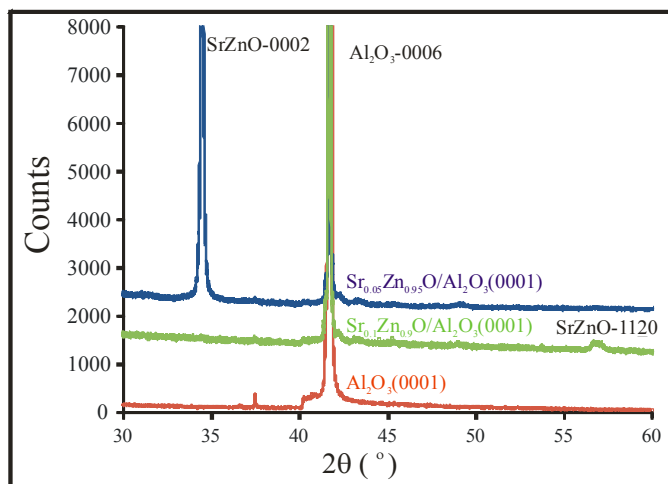


Fig. 7. XRD spectra of $\text{Al}_2\text{O}_3(0001)$ and $\text{Sr}_{0.05}\text{Zn}_{0.95}\text{O}$, and $\text{Sr}_{0.1}\text{Zn}_{0.9}\text{O}$ grown on $\text{Al}_2\text{O}_3(0001)$ at $T = 750^\circ\text{C}$ under 0.5 Torr O_2 background pressure

The earlier studies have shown that the ZnO doped structures are able to show some phase transitions [32]. One of the reasons is connected with occurrence of the anharmonic phonons [33]. This phonons form charge induced mechanical stresses [34]. At the same time there occurs some charge transfer forming the effects described by the third rank polar effects like SHG [35-36]. It may be even manifested in the ZnO containing glasses [37-39]. So the observed structural phase transitions may reflect a complex interaction of phonons and the electronic subsystem which finally determined the observed charge density acentricity effects.

4. Conclusions

A structural transition for the SrZnO alloy films from a wurtzite to a rock-salt structure, leading to a reduction in the (11 $\bar{2}$ 0)/(0001) surface energy ratio. The effect of substrate temperature and oxygen pressure during growth by PLD on the structural properties of SrZnO films was investigated. Different SrZnO films with $\text{SrO}/(\text{SrO} + \text{ZnO}) \leq 0.25$ were grown at different SrO ratios. XRD results indicated an improvement in the films' crystallinity as the temperature and O_2 pressure increased, up to 650°C and 0.5 Torr for the (0001) orientation. However, the crystallinity was reduced as the SrO content in the films

increased, whereas the magnitude of the c -lattice constants of these films showed a slight increase with increasing SrO content. Both optical measurements and SEM imaging explained the effect of SrO percentage on growth mode. Lastly, increasing the substrate temperature to 750°C resulted in a sharp (0002) peak at low SrO content (5%), and a virtually non-crystalline film with small crystallites adopting a (11 $\bar{2}$ 0) orientation was observed at higher SrO content (10%).

Acknowledgement

The authors would like to acknowledge the Saudi National Plan for Science, Technology, and Innovation (NPSTI), Saudi Arabia, for supporting this work under project No. 10-NAN1197-02.

REFERENCES

- [1] B. Santoshkumar, S. Kalyanaraman, R. Vettumperumal, R. Thangavel, Structure-dependent anisotropy of the photoinduced optical nonlinearity in calcium doped ZnO nanorods grown by low cost hydrothermal method for photonic device applications, *J. Alloys Compd.* **658**, 435-439 (2016).
- [2] L.N. Bai, J.S. Lian, W.T. Zheng, O. Jiang, First-principles study of optical properties in Ca-doped ZnO alloys, *Eur. J. Phys.* **10** (5), 1144-1149 (2012).
- [3] D.J. Cohen, K.C. Ruthe, S.A. Barnett, Transparent conducting $\text{Zn}_{1-x}\text{Mg}_x\text{O}$: (Al, In) thin films, *J. Appl. Phys.* **96** (1), 459-467 (2004).
- [4] T. Gruber, C. Kirchner, R. Kling, F. Reuss, A. Waag, ZnMgO epilayers and ZnO-ZnMgO quantum wells for optoelectronic applications in the blue and UV spectral region, *Appl. Phys. Lett.* **84** (26) 5359-5361 (2004).
- [5] T. Gruber, C. Kirchner, R. Kling, F. Reuss, A. Waag, F. Bertram, D. Forster, J. Christen & M. Schreck, Optical and structural analysis of ZnCdO layers grown by metalorganic vapor-phase epitaxy, *Appl. Phys. Lett.* **83** (16), 3290-3292 (2003).
- [6] H.A. Albrithen, A.M. El-Naggar, K. Ozga, H. Alshahrani, A. Alanazi, E. Alfaifi, J. Labis, et al., Giant increase of optical transparency for Zn-rich $\text{Ca}_x\text{Zn}_{1-x}\text{O}$ on $\text{Al}_2\text{O}_3(0001)$ grown by pulsed laser deposition, *Opt. Mater.* **52**, 1-5 (2016).
- [7] D.W. Ma, Z.Z. Ye, L.L. Chen, Dependence of structural and optical properties of $\text{Zn}_{1-x}\text{Cd}_x\text{O}$ films on the Cd composition, *Phys. Status Solidi A* **201**, 2929-2933 (2004).
- [8] T. Makino, C.H. Chia, N.T. Tuan, Y. Segawa, M. Kawasaki, A. Ohtomo, et al., Radiative and nonradiative recombination processes in lattice-matched (Cd,Zn)O/(Mg,Zn)O multiquantum wells, *Appl. Phys. Lett.* **77**, 1632-1634 (2000).
- [9] T. Makino, A. Ohtomo, C. Chia, Y. Segawa, H. Koinuma, M. Kawasaki, Internal electric field effect on luminescence properties of ZnO/(Mg, Zn)O quantum wells, *Physica E* **21**, 671-675 (2004).
- [10] T. Makino, Y. Segawa, M. Kawasaki, A. Ohtomo, R. Shiroki, K. Tamura, et al., Band gap engineering based on $\text{Mg}_x\text{Zn}_{1-x}\text{O}$ and $\text{Cd}_y\text{Zn}_{1-y}\text{O}$ ternary alloy films, *Appl. Phys. Lett.* **78**, 1237-1239 (2001).

- [11] T. Minemoto, T. Negami, S. Nishiwaki, H. Takakura, Y. Hamakawa, Preparation of $Zn_{1-x}Mg_xO$ films by radio frequency magnetron sputtering, *Thin Solid Films* **372**, 173-176 (2000).
- [12] K.P. Misra, R.K. Shukla, A. Srivastava, A. Srivastava, Blue shift in optical band gap in nanocrystalline $Zn_{1-x}Ca_xO$ films deposited by sol-gel method. *Appl Phys Lett* **95**, 031901 (2009)
- [13] K. Ogata, K. Koike, T. Tanite, T. Komuro, F. Yan, S. Sasa, et al., ZnO and ZnMgO growth on a-plane sapphire by molecular beam epitaxy, *J. Cryst. Growth* **251**, 623-627 (2003).
- [14] A. Ohtomo, M. Kawasaki, T. Koida, K. Masubuchi, H. Koinuma, Y. Sakurai, et al., $Mg_xZn_{1-x}O$ as a II–VI wide gap semiconductor alloy, *Appl. Phys. Lett.* **72**, 2466 (1998).
- [15] A. Ohtomo, M. Kawasaki, I. Ohkubo, H. Koinuma, T. Yasuda, Y. Segawa, Structure and optical properties of $ZnO/Mg_{0.2}Zn_{0.8}O$ superlattices, *Appl. Phys. Lett* **75**, 980-982 (1999).
- [16] A. Ohtomo, K. Tamura, M. Kawasaki, T. Makino, Y. Segawa, Z.K. Tang, G.K.L. Wong, Y. Matsumoto, H. Koinuma, Room-temperature stimulated emission of excitons in $ZnO/(Mg, Zn)O$ superlattices, *Appl. Phys. Lett* **77**, 2204-2206 (2000).
- [17] Y. Ryu, T.-S. Lee, J.A. Lubguban, H.W. White, B.J. Kim, Y.S. Park, et al., Next generation of oxide photonic devices: ZnO-based ultraviolet light emitting diodes, *Appl. Phys. Lett.* **88** (24), 241108 (2006).
- [18] Y.R. Ryu, T.S. Lee, J.A. Lubguban, A.B. Corman, H.W. White, J.H. Leem, et al., Wide-band gap oxide alloy: $BeZnO$, *Appl. Phys. Lett.* **88**, 052103 (2006).
- [19] K. Sakurai, T. Takagi, T. Kubo, D. Kajita, T. Tanabe, H. Takasu, et al., Spatial composition fluctuations in blue-luminescent $ZnCdO$ semiconductor films grown by molecular beam epitaxy, *J. Cryst. Growth* **237-239**, 514-517 (2002).
- [20] F.K. Shan, B.I. Kim, G.X. Liu, Z.F. Liu, J.Y. Sohn, W.J. Lee, et al., Blue shift of near band edge emission in Mg doped ZnO thin films and aging, *J. Appl. Phys.* **95**, 4772 (2004).
- [21] H.D. Sun, T. Makino, Y. Segawa, M. Kawasaki, A. Ohtomo, K. Tamura, H. Koinuma, Enhancement of exciton binding energies in $ZnO/ZnMgO$ multiquantum wells, *J. Appl. Phys.* **91**, 1993-1997 (2002).
- [22] O. Vigil, L. Vaillant, F. Cruz, G. Santana G, A. Morales-Acevedo, G. Contreras- Puente, Spray pyrolysis deposition of cadmium-zinc oxide thin films, *Thin Solid Films* **361**, 53-55 (2000).
- [23] Z.B. Ayadi, L. El Mir, J. El Ghoul, K. Djessas, S. Alaya, Structural and optical properties of calcium-doped zinc oxide sputtered from nanopowder target materials, *Int. J. Nanoelectron. Mater.* **3** (2), 87-97 (2010).
- [24] W. Water, S.F. Wang, Y.P. Chen, JCh Pu, Calcium and strontium doped ZnO films for love wave sensor applications, *Integr. Ferroelectr.* **72** (1), 13-22 (2005).
- [25] W. Water, Y.S. Yang, The influence of calcium doped ZnO films on Love wave sensor characteristics, *Sens. Actuators A: Phys.* **127**, 360-365 (2006).
- [26] P. Singh, Preparation and characterization of zinc-barium oxide composite, *J. Mater. Sci. Lett.* **9** (5), 613-615 (1990).
- [27] K. Uematsu, T. Morimoto, Z. Kato, N. Uchida, K. Sa'to, Solubility of barium oxide in zinc oxide, *J. Mater. Sci. Lett.* **6** (11), 1285-1286 (1987).
- [28] W. Water, T.H. Fang, L.W. Ji, T.H. Meen, Y.S. Yan, Surface morphology and liquid sensor sensitivity of barium-doped ZnO thin film, *J. Sci. Innov.* **1**(1), 25-32 (2011).
- [29] R. O'Hare, PhD thesis, Dublin City University, 2010.
- [30] Y. Duan, L. Qin, G. Tang, L. Shi, First-principles study of ground- and metastable-state properties of XO ($X=Be, Mg, Ca, Sr, Ba, Zn$ and Cd), *Eur. Phys. J. B.* **66**, 201-209 (2008).
- [31] S. Choopun, R.D. Vispute, W. Yang, R.P. Sharma, T. Venkatesan, H. Shen, Realization of band gap above 5.0 eV in metastable cubic-phase $Mg_xZn_{1-x}O$ alloy films, *Appl. Phys. Lett.* **80**, 1529-1531 (2002).
- [32] I.V. Kityk, J. Ebothe, A. El Hichou, Pressure-temperature anomalies of doped ZnO polycrystalline films deposited on bare glasses, *Mater. Lett.* **51** (6), 519-524 (2001).
- [33] I.V. Kityk, J. Ebothe, A. El Hichou, M. Addou, A. Bougrine, B. Sahraoui, Linear electro-optics effect in ZnO-F film-glass interface, *Phys. Status Solidi B* **234**, 553-562 (2002).
- [34] T.M. Williams, D. Hunter, A.K. Pradhan, I.V. Kityk, Photoinduced piezo-optical effect in Er doped ZnO films, *Appl. Phys. Lett.* **89**, 043116 (2006).
- [35] J. Ebothe, I.V. Kityk, S. Benet, B. Claudet, K.J. Plucinski, K. Ozga, Photoinduced effects in ZnO films deposited on MgO substrates, *Opt. Commun.* **268**, 269-272 (2006).
- [36] K. Ozga, T. Kawaharamura, A. Ali Umar, M. Oyama, K. Nouneh, A. Slezak, S. Fujita, et al., Second-order optical effects in Au nanoparticle-deposited ZnO nanocrystallite films, *Nanotechnology* **19**, 185709 (2008).
- [37] G. Lakshminarayana, J. Qiu, M.G. Brik, G.A. Kumar, I.V. Kityk, Spectral analysis of Er^{3+} , Er^{3+}/Yb^{3+} - and $Er^{3+}/Tm^{3+}/Yb^{3+}$ doped TeO_2 -ZnO- WO_3 - TiO_2 - Na_2O glasses, *J. Phys. - Condens. Mat.* **20**, 375101 (2008).
- [38] A. Douayar, M. Abd-Lefdil, K. Nouneh, P. Prieto, R. Diaz, A.O. Fedorchuk, I.V. Kityk, Photoinduced pockels effect in the Nd-doped ZnO oriented nanofilms, *Appl. Phys. B* **110**(3), 419-423 (2013).
- [39] B. Santoshkumar, S. Kalyanaraman, R. Vettumperumal, R. Thangavel, I.V. Kityk, S. Velumani, Structure-dependent anisotropy of the photoinduced optical nonlinearity in calcium doped ZnO nanorods grown by low cost hydrothermal method for photonic device applications, *J. Alloys Compd.* **658**, 435-439 (2016).